Optimal design of a heat exchanger for automotive thermoelectric generator systems applied to a passenger car

Ding Luo[a], Zihao Wu[a], Yuying Yan[b], Dongxu Ji[c,*], Ziming Cheng[d], Ruochen Wang[e], Ying Li[b], Xuelin Yang[a,*]

[a] College of Electrical Engineering & New Energy, China Three Gorges University, Yichang, China

[b] Faculty of Engineering, University of Nottingham, University Park, Nottingham, UK

[c] School of Science and Engineering, The Chinese University of Hong Kong, Shenzhen, China

[d] School of Energy Science and Engineering, Harbin Institute of Technology, Weihai, China

[e] School of Automobile and Traffic Engineering, Jiangsu University, Zhenjiang, China

Corresponding authors: *xlyang@ctgu.edu.cn; * jidongxu@cuhk.edu.cn

Abstract: The heat exchanger determines the overall performance of automotive thermoelectric generator (ATEG) systems. To obtain the accurate performance of the ATEG system under actual driving conditions, a fluid-thermal-electric multiphysics numerical model is established. Considering the backpressure loss, weight loss, and pumping power loss, a net power model of the ATEG system is established. The performance of the two heat exchangers with and without fins is investigated and compared. Through optimizations, the optimal parameters for the heat exchanger with fins are N_W = 2 rows, H = 30 mm, and N_L = 5 columns, and those of the heat exchanger without fins are N_W = 2 rows, H = 10 mm, and N_L = 4 columns. The output power, net power, conversion efficiency, and net efficiency of the optimal ATEG system with fins are 35.49 W, 22.93 W, 1.89%, and 1.22%, respectively, and those of the optimal ATEG system without fins are 16.49 W, 8.67 W, 1.51%, and 0.79%, respectively. Through the use of fins, the net power and net efficiency of the ATEG system can be increased by 164.48% and 54.43% respectively. The results are helpful to guide the optimization and design of ATEG systems.

Keywords: heat exchanger; automotive thermoelectric generator; numerical model; net power; optimization.

Nomenclature

Symbols

A	area, m^2
c	specific heat, $J \cdot kg^{-1} \cdot K^{-1}$
$\vec{E}$	electric field density vector, $V \cdot m^{-2}$
f	rolling resistance coefficient
H	height, mm
$\vec{J}$	current density vector, $A \cdot m^{-2}$
k	turbulent kinetic energy, $m^2 \cdot s^{-2}$
$\dot{m}$	mass flow rate, $g \cdot s^{-1}$
N	number
p	pressure, Pa
P	power, W
Q	heat absorption, W
R	resistance, Ω
$\dot{S}$	source term
T	temperature, K
U	output voltage, V
v	velocity, $m \cdot s^{-1}$
$\dot{V}$	volume flow rate, $m^3 \cdot s^{-1}$
W	weight, N

Greek symbols

α	Seebeck coefficient, $\mu V \cdot K^{-1}$
σ	electrical conductivity, $S \cdot m^{-1}$
ϕ	electrical potential, V
ε	turbulent dissipation rate, $m^2 \cdot s^{-3}$
ρ	density, $kg \cdot m^{-3}$
μ	dynamic viscosity, Pa·s
λ	thermal conductivity, $W \cdot m^{-1} \cdot K^{-1}$
η	conversion efficiency
γ	Voltage uniformity coefficient

Subscripts

ave	average
b	backpressure loss
co	copper electrodes
ex	exhaust gas
exi	exhaust inlet
exo	exhaust outlet
h	hot side
i	ith, i = 1, 2, 3, ……
L	length or load resistance
m	material
n	n-type legs
net	net power or net efficiency
out	output power
p	n-type legs or pumping power loss
t	transmission system
v	vehicle
W	width
w	weight loss

Abbreviations

ATEG	automotive thermoelectric generator
CFD	computational fluid dynamics
HWFET	highway fuel economy test
SUV	sports utility vehicle
TEG	thermoelectric generator
TEM	thermoelectric module

1. Introduction

Thermoelectric power generation technology has aroused great interest in harvesting waste heat from the automotive exhaust gas, because of the unparalleled merits of no moving parts, no emissions, no maintenance costs, silent operation, and long service life [1-3]. When the thermoelectric generator (TEG) is applied to waste heat recovery from an automotive diesel engine, it has the potential of producing over 1000 W of electricity [4], fully satisfying the power demand of on-vehicle equipment. Through designing a recycling circuit controller [5], the produced energy can be directly used for the power supply of lights, audios, etc., or stored in vehicle batteries. Accordingly, the vehicle fuel consumption rate is reduced. The potential fuel saving produced by the automotive TEG system is

about 6% [6]. However, the conversion efficiency of existing automotive thermoelectric generator (ATEG) systems to convert the absorbed waste heat into electrical energy is generally less than 4% [7-9]. To achieve the wide application of the TEG in automotive waste heat recovery, its conversion efficiency needs a further breakthrough.

The ATEG system is composed of a heat exchanger structure, thermoelectric module (TEM) arrays, and a cooling structure. Generally, there are numerous different types of heat exchangers used in ATEG systems, such as plate type [10], polygonal type [11], and cylindrical type [12]. For the plate-type heat exchanger, the TEM array is arranged on the two hot end surfaces [13], which has the advantages of simple structure and flexible fin configurations. For the polygonal heat exchanger, it can apply more TEMs due to multiple hot-side surfaces and can be integrated with other exhaust systems such as muffler [14] and catalytic converter [15]. Only a few studies [16] have studied the cylindrical heat exchanger because the TEM needs to be designed with a ring shape to fit the curved hot end surface of the heat exchanger, which requires high cost. From light-duty passenger cars to heavy-duty commercial vehicles, the mass flow rate of exhaust gas produced by combustion engines under a dynamic driving cycle ranges from ~10 g/s [17] to ~300 g/s [18]. Accordingly, to adapt to high or low mass flow rate applications, the plate-type heat exchanger can respectively increase or decrease the number of plates, while a polygonal heat exchanger can respectively increase or decrease the number of edges. For a mass flow rate of 71.5 g/s, Wang et al. [19] divided the exhaust manifold into four channels and proposed a four-ATEG system to maximize waste heat recovery, wherein each ATEG unit was plate-type and equipped with 60 TEMs. In addition to dividing the exhaust manifold into multiple channels, the plate-type heat exchanger can be stacked with TEM arrays and cooling devices to form a multi-layer design to recover the exhaust heat with a high mass flow rate.

To determine the optimal cross-section shape of the heat exchanger, Yan et al. [20] compared the performance of ATEG systems with different cross-section shapes and reported that the rectangular-shaped channel produces the highest power generation and conversion efficiency. Accordingly, this paper focuses on the optimal design of a plate-type heat exchanger. High heat transfer performance and low-pressure drop are two criteria to evaluate the performance of heat exchangers. Fernández-Yañez et al. [21] proposed a ratio of heat absorption to backpressure loss to compare the performance of four heat exchangers, in which the internal flow channels were mounted with long fins, two kinds of short-fin designs with different mixes, and channel-arranged fins, respectively. According to computational fluid dynamics (CFD) results, the long-fin design can achieve the highest ratio. Also, some novel optimization approaches were suggested to enhance the performance of plate-type heat

exchangers. Cao et al. [22] and Pacheco et al. [23] introduced heat pipes into the heat exchanger for automotive exhaust heat recovery and pointed out that the heat pipe assisted heat exchanger has a good potential for high thermal load applications. A great number of researches on the structure optimization of plate-type heat exchangers have been reported. However, there are no comprehensive optimization and design strategies for the plate-type heat exchanger of the ATEG system.

The performance evaluation method of the ATEG system is the premise of designing and optimizing heat exchangers. CFD model plays an important role in the structural optimization of heat exchangers [24, 25]. However, the electric performance of the ATEG system can not be estimated by the CFD model. For this issue, Chen et al. [26] used the average surface temperature data obtained from CFD simulations as the working temperature of TEMs to calculate the output power and conversion efficiency of the ATEG system. To make the predicted results more accurate, Luo et al. [27] proposed a fluid-thermal-electric multiphysics model to evaluate the performance of a gas-to-water TEG system. Compared with the traditional analytical model, the predicted results of the proposed model were more reasonable [28]. Nevertheless, the used gas-to-water TEG system only contained one TEM, which was not in line with the actual situation of ATEG systems, as well as the fluid, thermal, and electric fields were not solved simultaneously in the model, resulting in errors. Therefore, it is necessary to establish a comprehensive fluid-thermal-electric multiphysics model of the ATEG system to guide the performance analysis and structure design.

As mentioned above, the plate-type heat exchanger exhibits good heat transfer performance and is widely used in ATEG systems. However, the mass flow rate of different vehicles varies greatly. For a specific ATEG system, when applied to light-duty vehicles, the exhaust gas generated can not fill the exhaust channel, resulting in low heat transfer efficiency. When used in heavy-duty vehicles, the exhaust gas generated may overfill the exhaust channel and cause excessive backpressure. At present, there are no comprehensive optimization and design strategies for the plate-type heat exchanger of the ATEG system. For this reason, this work tries to explore the optimal parameters of the plate-type heat exchanger for thermoelectric waste heat recovery of a passenger car, including the height, width, and length, to maximize the energy utilization from waste heat. Besides, a comprehensive fluid-thermal-electric multiphysics model for ATEG systems is established to predict the electric performance of the ATEG system under different structural parameters of the plate-type heat exchanger.

This work fills the gap about how to select the optimal parameters of the plate-type heat exchanger of the ATEG system for a specific vehicle, and how to predict the performance of the ATEG system with high reasonability. Considering the effect of fin structure on the heat exchanger, two plate-type

heat exchangers with and without fins are studied. The layout of this paper is as follows: Section 2 introduces the model in detail. Section 3 discusses the numerical results under different heat exchanger parameters. Section 4 analyzes the optimal design of the plate-type heat exchanger. Section 5 summarizes the main findings of this study.

2. Model description

2.1 Diagram of the automotive thermoelectric generator system

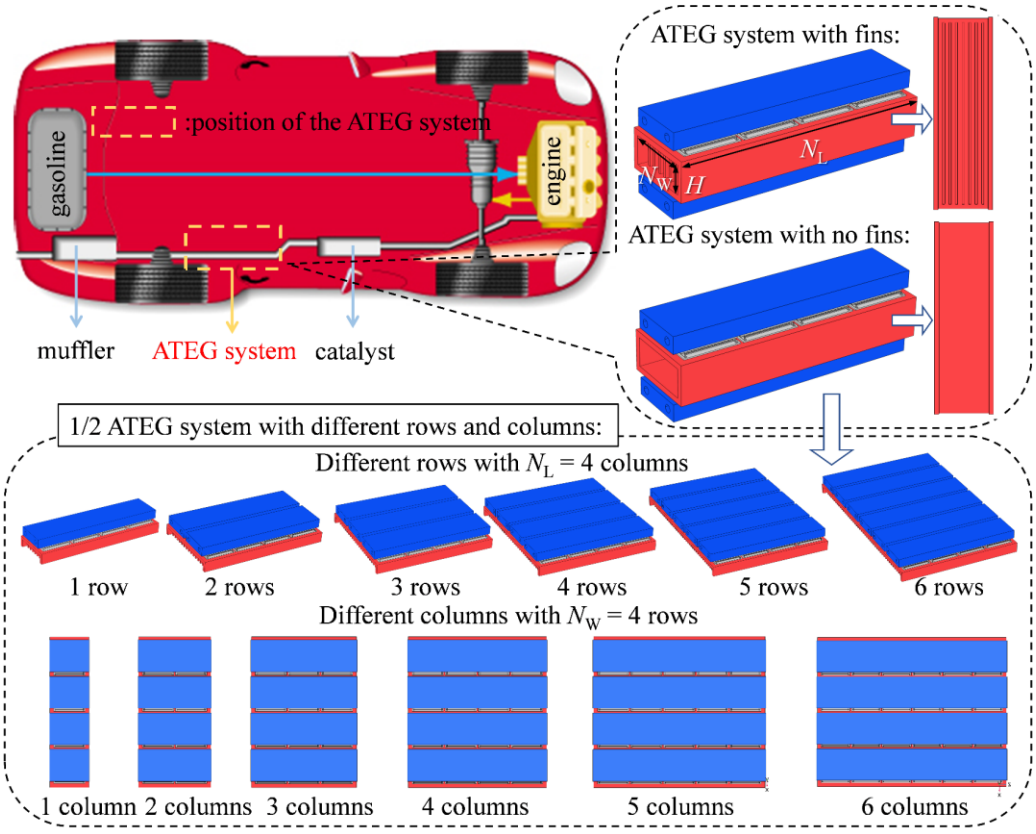

Fig. 1. Position of the ATEG system in a passenger car and the diagram of the ATEG system with different configurations.

The heat transfer performance of the heat exchanger determines the overall performance of the ATEG system. To guide the design of the ATEG system and ensure its high performance, the height, width, and length of the plate-type heat exchanger are comprehensively optimized. Besides, the ATEG system is used to recover exhaust heat from a given passenger car. When the optimized ATEG system is applied from passenger cars to heavy trucks or other large-size vehicles, it can be regarded as one of the subsystems like Ref. [19] in which the exhaust gas was divided into several parts through the manifold and flows through each subsystem respectively, or it can be designed as a multi-layer structure like Ref. [29], to ensure the high efficiency of the optimized ATEG system. The number of

subsystems and the number of layers of the multi-layer structure are determined according to the integer multiple relationships of the exhaust mass flow rate between the large-size vehicle applied and the passenger car given herein.

Here, the height of the heat exchanger can be adjusted at will, however, its width and length must be an integral multiple of the corresponding size of the TEM. To ensure high heat transfer performance, the heat exchanger and heat sink are made of aluminium materials with thermal conductivity of 201 W/(m·K). The Bi_2Te_3-based commercial TEM (TEG-127020, P&N Technology, China) is used as the power generation unit, and its structural size and material properties are listed in Table 1 [30]. The TEM consists of 256 copper electrodes, 128 pairs of thermoelectric legs, and two ceramic plates. Considering the layout gap between TEMs, the width and length of the basic unit of the ATEG system are set as 46 mm and 42 mm respectively. Fig. 1 shows the position of the ATEG system in a passenger car and the diagram of the ATEG system with different configurations. The ATEG system is located between the muffler and the catalyst of the passenger car. The height (H) varies at a value of every 5 mm from 5 mm to 30 mm. The width (N_W) varies from 1 row to 6 rows. The length (N_L) varies from N_L = 1 column to N_L = 6 columns. To reduce the computing time and workload, the 1/2 ATEG system is used as the research objective to analyze the performance of the complete ATEG system. The symmetrical surface is defined on the middle plane of the heat exchanger. Consequently, the height (H) varies at a value of every 2.5 mm from 2.5 mm to 15 mm in the 1/2 ATEG system. According to the optimization results of previous research [31], a water-based heat sink with a pipeline diameter of 5.5 mm is adopted to ensure good cooling performance. Also, the size and number of heat sinks correspond to the heat exchanger.

Table 1. Datasheet of the Bi_2Te_3-based TEM [30].

	Seebeck coefficient ($\mu V \cdot K^{-1}$)	Thermal conductivity ($W \cdot m^{-1} \cdot K^{-1}$)	Electrical resistivity (10^{-5}ohm·m)	Size (L×W×H mm^3)
p-type legs	$-1.80268\times10^{-7}T^4 +3.23632\times10^{-4}T^3-0.21537T^2 +62.97444T-6616.56781$	$-3.05948\times10^{-9}T^4 +4.56781\times10^{-6}T^3-2.51621\times10^{-3}T^2 +0.61074T-53.98632$	$-3.08802\times10^{-9}T^4 +4.56531\times10^{-6}T^3-2.58541\times10^{-3}T^2 +0.65579T-60.58804$	1.4×1.4×1
n-type legs	$1.80268\times10^{-7}T^4 -3.23632\times10^{-4}T^3+0.21537T^2 -62.97444T+6616.56781$	$-3.05948\times10^{-9}T^4 +4.56781\times10^{-6}T^3-2.51621\times10^{-3}T^2 +0.61074T-53.98632$	$-3.08802\times10^{-9}T^4 +4.56531\times10^{-6}T^3-2.58541\times10^{-3}T^2 +0.65579T-60.58804$	1.4×1.4×1
copper electrodes	-	165.64	1.75×10^{-3}	3.8 × 1.4× 0.35
ceramic plates	-	22	-	40 × 44 (and 40) × 0.8

When the length of the heat exchanger is fixed at a specific value (N_L = 4 columns in this study), the optimization for the height and width is carried out at the same time, because both will affect the cross-sectional area of the exhaust channel. After determining the optimal height and width, the optimization for length is performed. Considering the great influence of fins on the heat exchanger, the two kinds of heat exchangers with and without fins are studied. According to Ref. [32], the plate-fin structure provides better performance than other fin structures, and thus plate fins are adopted for the heat exchanger with fins. Also, the thickness of fins and the spacing between them are set as 2 mm and 4 mm respectively, according to the optimization results of Ref. [33]. There are 7 plate fins for a basic unit of the ATEG system. As for the heat exchanger with no fins, it has a smooth exhaust gas channel.

2.2 Governing equations of the comprehensive fluid-thermal-electric multiphysics numerical model

In the subsequent numerical simulation, the following preconditions are made:

(i) Thermoelectric materials are isotropic.

(ii) The contact thermal resistance between TEM and other components is neglected because its influence can be minimized by applying thermal grease and applying clamping force [34], and the contact thermal resistance is often ignored in previous studies [35]. Through preliminary analysis, the power difference between the ATEG with and without consideration of contact thermal resistance [36] is within 2%, which indicates that the contact thermal resistance plays an insignificant role in the overall performance of the ATEG.

(iii) Dry air is taken as exhaust gas and water as coolant.

(iv) Heat radiation is also ignored due to its tiny influence.

The governing equations of the comprehensive fluid-thermal-electric multiphysics numerical model can be divided into three parts: fluid domain, thermal conduction domain, and thermal-electric conversion domain. For the fluid domain, the fluid flow can be characterized by CFD equations [37], as follows:

$$\nabla \cdot \vec{v} = 0 \tag{1}$$

$$\nabla \cdot \left(\vec{v}\vec{v}\right) = -\frac{1}{\rho}\nabla p + \nabla \cdot \left(\mu \nabla \vec{v}\right) \tag{2}$$

$$\nabla \cdot \left(\lambda \nabla T\right) = \rho c \vec{v} \cdot \nabla T \tag{3}$$

where, $\vec{v}$ is the vector of fluid velocity, p is the fluid pressure, T is the absolute temperature. ρ, μ, λ, and c are the interior properties of fluids, which denotes the density, molecular viscosity, thermal conductivity, and specific heat, respectively.

In addition, the fluid flow in the exhaust gas channel of the heat exchanger and the cooling water channel of the heat sink can be viewed as turbulence. To compute the flow field, the standard *k*-ε turbulence model [38] is adopted in this study, which transport equations include:

$$\rho\left(\vec{v}\cdot\nabla\right)k=\nabla\cdot\left[\left(\mu+\frac{\mu_t}{\sigma_k}\right)\nabla k\right]+P_k-\rho\varepsilon \tag{4}$$

$$\rho\left(\vec{v}\cdot\nabla\right)\varepsilon=\nabla\cdot\left[\left(\mu+\frac{\mu_t}{\sigma_\varepsilon}\right)\nabla\varepsilon\right]+C_{1\varepsilon}\frac{\varepsilon}{k}P_k-C_{2\varepsilon}\rho\frac{\varepsilon^2}{k} \tag{5}$$

with

$$\mu_t=\rho C_\mu\frac{k^2}{\varepsilon} \tag{6}$$

where k and ε are the turbulence kinetic energy and the dissipation rate of turbulence energy respectively. P_k is the shear production of turbulence kinetic energy. $C_{1\varepsilon}$, $C_{2\varepsilon}$, C_μ, σ_k, and σ_ε are constants defined as $C_{1\varepsilon}$ = 1.44, $C_{2\varepsilon}$ = 1.92, C_μ = 0.09, σ_k = 1.0, and σ_ε = 1.3 [39].

In the thermal conduction domain, including the heat exchanger and heat sink, the energy conservation equation is defined as:

$$\nabla\cdot\left(\lambda\nabla T\right)=0 \tag{7}$$

In the thermal-electric conversion domain, including the TEM and load resistance, its energy conservation can be written as:

$$\nabla\cdot\left(\lambda_\mathrm{m}\nabla T\right)+\dot{S}_\mathrm{m}=0 \tag{8}$$

where, subscript m represents the name of different materials, ce for ceramic plates, co for copper electrodes, n for n-type thermoelectric legs, p for p-type thermoelectric legs, L for load resistance. $\dot{S}_m$ is the energy source term in different computational regions, which is [40]:

$$\dot{S}_\mathrm{m}=\begin{cases}\sigma_\mathrm{p}^{-1}\left(T\right)\vec{J}^2-\nabla\alpha_\mathrm{p}\left(T\right)\vec{J}T_\mathrm{p}; & \text{p-type thermoelectric leg}\\ \sigma_\mathrm{n}^{-1}\left(T\right)\vec{J}^2-\nabla\alpha_\mathrm{n}\left(T\right)\vec{J}T_\mathrm{n}; & \text{n-type thermoelectric leg}\\ \sigma_\mathrm{co}^{-1}\vec{J}^2; & \text{copper electrode}\\ \sigma_\mathrm{L}^{-1}\vec{J}^2; & \text{load resistance}\\ 0; & \text{ceramic plates}\end{cases} \tag{9}$$

where, σ^{-1} is the electrical resistivity, $\vec{J}$ is the current density vector, α is the Seebeck coefficient. It is worth noting that the thermal conductivity, electrical resistivity, and Seebeck coefficient of

thermoelectrical materials are temperature-dependent.

Besides the energy conservation equation, the computational domain of current flow, including copper electrodes, load resistance, p-type and n-type thermoelectric legs, also follows the governing equations of the electric field, as follows [41]:

$$\vec{E} = -\nabla\phi + \alpha_{\mathrm{p,\,n}}\left(T\right)\nabla T \tag{10}$$

$$\vec{J} = \sigma_{\mathrm{m}}\vec{E} \tag{11}$$

$$\nabla \cdot \vec{J} = 0 \tag{12}$$

where, $\vec{E}$ and ϕ are the electrical field density vector and electrical potential respectively. The last term in Eq. (10) represents the generated voltage due to the Seebeck effect. The continuity of current is expressed by Eq. (12).

Eqs (1)-(12) constitute the governing equations of the comprehensive fluid-thermal-electric multiphysics numerical model. Combined with boundary conditions, the model can be calculated by numerical analysis methods, such as the finite element method [42].

2.3 Vehicle parameters and boundary conditions

To calculate the above numerical model, reasonable boundary conditions are needed, including the boundary conditions of the fluid, thermal, and electric fields. Herein, the exhaust temperature and mass flow rate are used as the inlet boundary conditions of the exhaust channel. In this study, the ATEG system is designed and optimized for a passenger car. The actual operation condition of the selected vehicle is simulated by ADVISOR [43], a professional vehicle simulation package. Table 2 lists the key parameters of the passenger car in the simulation environment, and the vehicle is set to run under HWFET (Highway fuel economy test) driving cycles.

Table 2. Key parameters of the passenger car.

Parameter	Value	unit
vehicle type	passenger car	-
engine type	gasoline engine	-
maximum engine power	102×10^3	W
engine displacement	3	L
number of cylinders	6	-
cargo	250×10^3	g
total mass	1747×10^3	g

According to the simulation results of ADVISOR, the exhaust temperature and mass flow rate are extracted from the exhaust gas after the catalyst [44]. Fig. 2 shows the time-dependent exhaust temperature, exhaust mass flow rate, and vehicle speed of the passenger car under the HWFET driving

cycle. Accordingly, the average values of 546.73 K and 18.24 g/s are used as the inlet conditions of the exhaust channel. In the coolant channel, the inlet temperature of 300 K and inlet velocity of 1 m/s are defined. On the outlet surfaces of both exhaust and coolant channels, a pressure outlet with a standard atmospheric pressure is defined. On the surfaces of the ATEG system exposed to the environment, a heat loss boundary condition with a convection coefficient of 15 W/(m^2·K) and an environmental temperature of 300 K [45] is adopted. As for the electric field, it only needs the grounded boundary condition, that is, the potential of the TEM terminal with a p-type leg is set to 0 V. Besides, to reduce the execution time, only 1/2 of the ATEG system is considered, and the symmetric boundary condition is adopted on the symmetry plane. For the 1/2 ATEG system, the exhaust mass flow inlet should be divided by 2, which is 9.12 g/s.

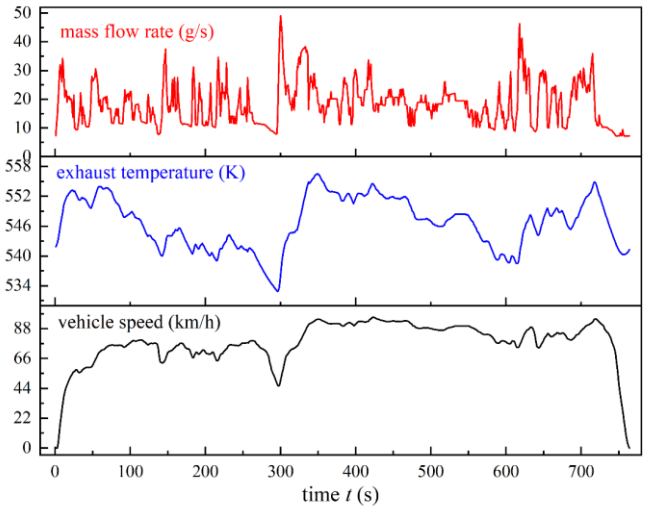

Fig. 2. Exhaust temperature and exhaust mass flow rate under the HWFET driving cycle.

2.4 Optimal load resistance of the TEM

Owing to the temperature dependence of thermoelectric material properties, the internal resistance of the TEM varies with the working temperature [46]. Determining the optimal load resistance of the TEM is the premise of numerical simulations of the ATEG system. In the ATEG system, all TEMs have the same size (40×40×3.3 mm^3) and parameters. Through the preliminary numerical simulations, it is found that the hot-side temperature of the TEM for the ATEG system with different heat exchanger configurations fluctuates in the range of 400-500 K. Taking a single TEM as the research objective, the output power of the TEM at different working temperatures is predicted by using a thermal-electric numerical model [47]. Fig. 3 shows a schematic diagram of the TEM and its output power at different working temperatures. Regardless of the change in the hot-side temperature (T_h), it can be observed

that the optimal load resistance of the TEM is about 4 Ω. Therefore, the load resistance of each TEM is set to 4 Ω during simulations.

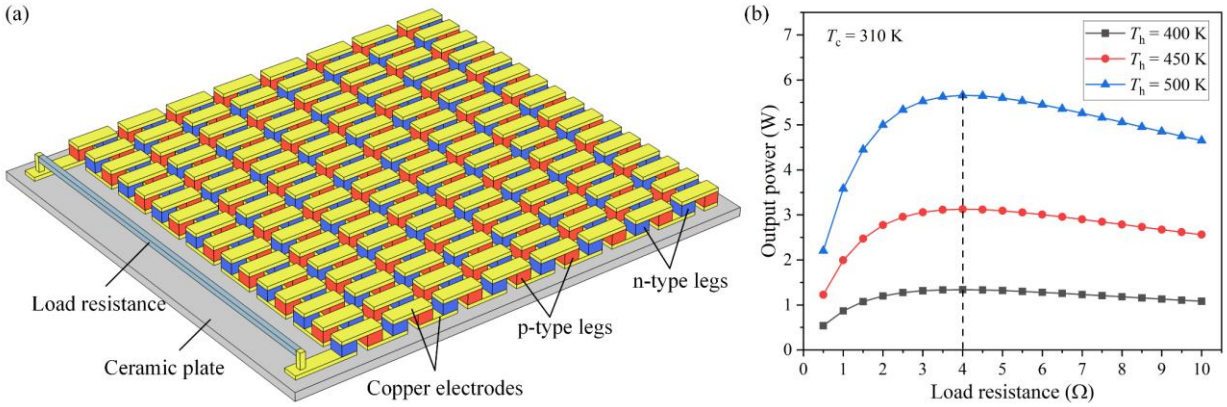

Fig. 3. Schematic diagram of the TEM and its output power at different working temperatures.

2.5 Finite element model and grid independence examination of the ATEG system

The model is numerically calculated by the finite element method on the platform of COMSOL Multiphysics [48]. Fig. 4 shows the finite element model of the ATEG system, in which, H = 10 mm, N_W = 1 row, and N_L = 4 columns. To balance the calculation accuracy and time, a grid independence examination for the finite element model is performed. The four cases with 1474662, 807467, 401389, and 218453 grids in the ATEG system are designated as case I, case II, case III, and case IV, respectively. Taking the output voltage of the first TEM under case I as the reference, the errors of case II, case III, and case IV are 0.28%, 0.85%, and 2.66%, respectively. Also, the time consumption from case I to case IV is greatly reduced. Therefore, case III with 401389 grids is used for the following simulations.

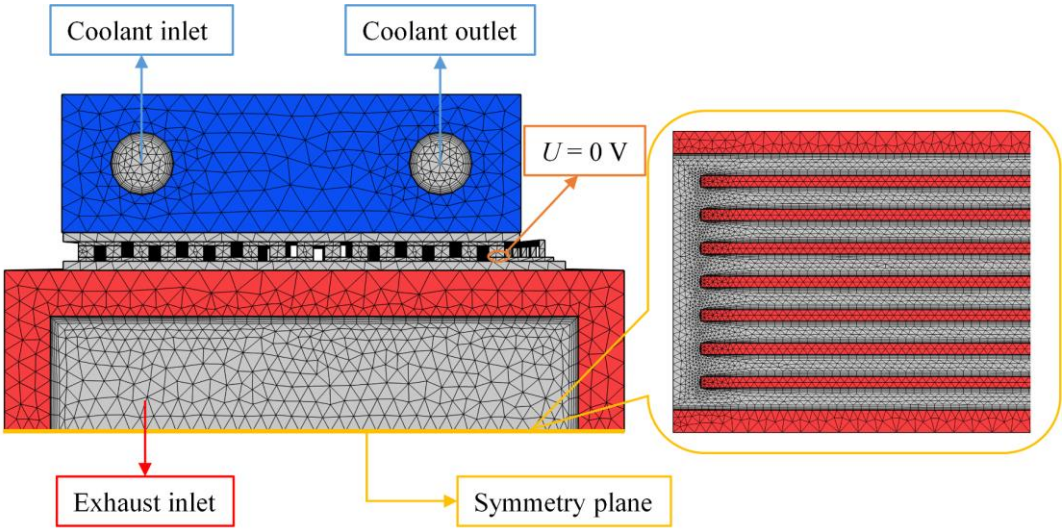

Fig. 4. Finite element model of the ATEG system.

2.6 Parameter definitions

Output power and conversion efficiency of the ATEG system are two key indexes to measure its performance. The output power of the ATEG system can be regarded as the sum of the output power of all TEMs, that is [10]:

$$P_{\text{out}} = \sum_{i=1}^{n} P_{\text{i}} = \sum_{i=1}^{n} \frac{U_{\text{i}}^2}{R_{\text{L}}} \tag{13}$$

where, P_{out} is the output power of the ATEG system, subscript i = 1, 2, 3,…, n denotes ith TEM, P_{i} is the output power of ith TEM, U_{i} is the output voltage of ith TEM, and R_{L} = 4 Ω is the load resistance, respectively.

The conversion efficiency of the ATEG system is equal to the output power divided by the heat absorbed from exhaust gases, which is defined by [49]:

$$\eta = \frac{P_{\text{out}}}{Q_{\text{h}}} = \frac{P_{\text{out}}}{c_{\text{ex}} \dot{m}_{\text{ex}} \left(T_{\text{exi}} - T_{\text{exo}} \right)} \tag{14}$$

where, η is the conversion efficiency of the ATEG system, Q_{h} is the heat absorbed from exhaust gases, subscript ex denotes exhaust gases, $\dot{m}$ is the mass flow rate, T_{exi} and T_{exo} are the exhaust inlet and outlet temperatures, respectively.

However, the ATEG system not only brings energy gains to the vehicle but also produces additional energy losses. The energy losses include weight loss, pumping power loss, and backpressure loss. Herein, the net power of the ATEG system is defined by [29]:

$$P_{\text{net}} = P_{\text{out}} - P_{\text{w}} - P_{\text{b}} - P_{\text{p}} \tag{15}$$

where, P_{w}, P_{b}, and P_{p} are the weight loss, backpressure loss of the exhaust gas, and pumping power loss of the cooling water, respectively.

The weight loss represents the additional vehicle power required to drive the ATEG system, which is [29]:

$$P_{\text{w}} = \frac{f v_{\text{v}}}{\eta_{\text{t}}} W_{\text{ateg}} \tag{16}$$

where, f = 0.012 represents the rolling resistance coefficient, v_{v} = 77.65 km/h represents the average vehicle speed under an HWFET driving cycle, η_{t} = 0.9 represents the transmission efficiency of the vehicle drivetrain system, and W_{ateg} is the weight of the ATEG system, respectively. The corresponding vehicle parameters are obtained from the vehicle model in ADVISOR.

When the exhaust gas flows through the heat exchanger, there is a pressure drop from the exhaust

inlet to the exhaust outlet, which can be characterized by backpressure loss [29]:

$$P_{\mathrm{b}} = \dot{V}_{\mathrm{ex}} \Delta p_{\mathrm{ex}} = \frac{\dot{m}_{\mathrm{ex}}}{\rho_{\mathrm{ex}}} \Delta p_{\mathrm{ex}} \tag{17}$$

where, $\dot{V}$ is the volume flow rate, Δp is the pressure drop, $\dot{m}$ is the mass flow rate, and ρ is the density, respectively.

Similarly, the pumping power loss can be written as [29]:

$$P_{\mathrm{p}} = \dot{V}_{\mathrm{wa}} \Delta p_{\mathrm{wa}} = v_{\mathrm{wa}} A_{\mathrm{wa}} \Delta p_{\mathrm{wa}} \tag{18}$$

where, subscript wa denotes the cooling water, v_{wa} is the fluid velocity of the cooling water, and A_{wa} is the cross-sectional area of the cooling water channel, respectively.

In addition, the net conversion efficiency of the ATEG system can be written as:

$$\eta_{\mathrm{net}} = \frac{P_{\mathrm{net}}}{Q_{\mathrm{h}}} \tag{19}$$

2.7 Experimental validation of the model

The experimental results in Ref. [27] are used to verify the model. According to the parameters in their study, the finite element model of the TEG system is established and the numerical calculation is carried out. Fig. 5 shows a comparison of the output voltage and power between the predicted and experimental data. The average errors of output voltage and power are 1.42% and 2.81% respectively. The developed model is proven to be able to accurately predict the performance of TEG systems under real conditions, and then guide the optimization of the TEG system.

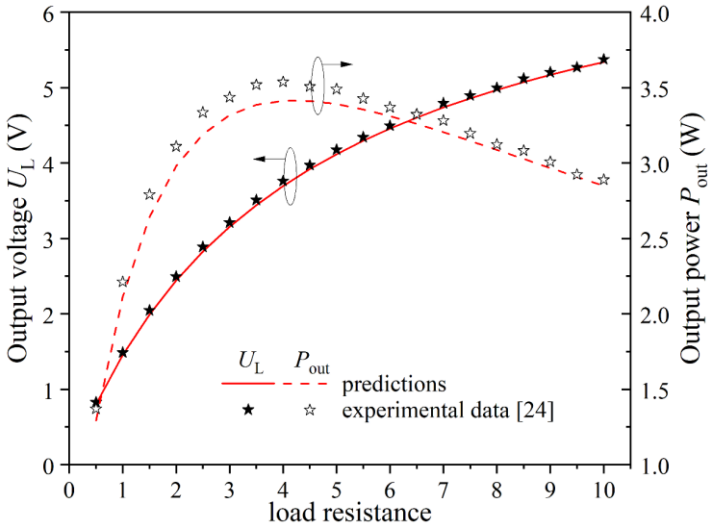

Fig. 5. Model validation using experimental data in [27].

3. Physical field distribution characteristics of the ATEG system

In this section, taking an ATEG system with H = 15 mm, N_W = 1 row, and N_L = 4 columns as the objective, the distribution characteristics of the ATEG system are elucidated in detail, and the performance can be observed from these distributions. Besides, the fin structure has a serious impact on the heat exchanger and then affects the overall performance of the ATEG system.

3.1 Temperature distributions

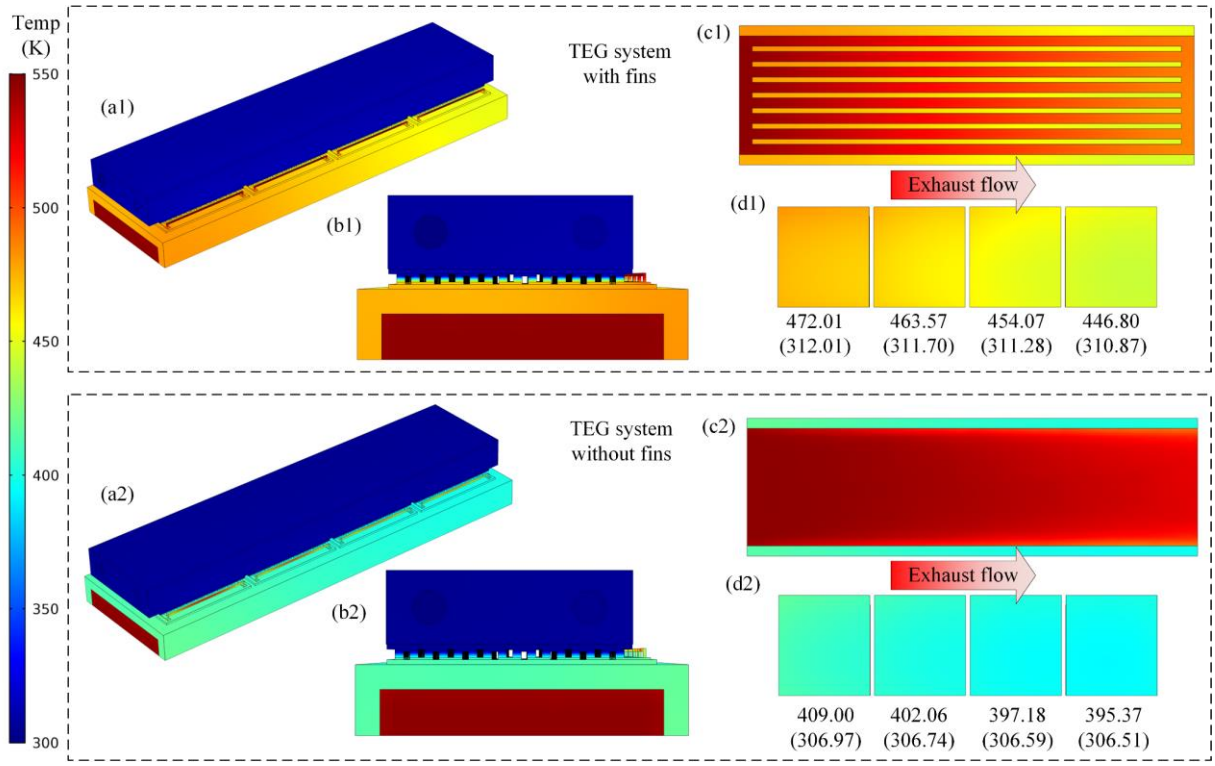

Fig. 6. Temperature distributions of the ATEG system. (a1), (b1), and (c1) are the main, side, and bottom-side views of temperature distributions of the ATEG system with fins, respectively; (a2), (b2), and (c2) are the main, side, and bottom-side views of temperature distributions of the ATEG system without fins, respectively; (d1) and (d2) are the TEM hot (cold) -side temperature distributions of the ATEG system with and without fins respectively.

Fig. 6 shows the temperature distributions of the ATEG system. Under the same conditions, the heat exchanger temperature of the ATEG system with fins is higher than that of the ATEG system without fins. Owing to the use of fins, the heat transfer area of the heat exchanger increases, the convective heat transfer is significantly enhanced, and more heat from the exhaust gas is collected by the finned heat exchanger. Designing a high-performance fin structure is one of the effective ways to improve the performance of ATEG systems. Besides, temperature drops can be observed from both directions from the exhaust inlet to the exhaust outlet and from the exhaust gas to the cooling water. In the

direction of heat conduction from the exhaust gas to the cooling water, the temperature drop from the hot side to the cold side of TEMs accounts for 64.85% of the total temperature drop in the ATEG system with fins, whereas that is 41.35% in the ATEG system without fins. In the downward flow direction of the exhaust gas, the TEM hot-side temperature drop from the first TEM to the fourth TEM is 25.21 K in the ATEG system with fins, whereas that is 13.63 K in the ATEG system without fins. The heat contained in the exhaust gas is absorbed by the heat exchanger, then transferred to the TEM, and finally dissipated by the cooling water. Part of the heat absorbed by the TEM is converted into electricity. For this reason, as the exhaust gas flows downward, the heat contained in the exhaust gas gradually decreases, especially in the ATEG system with fins.

Moreover, the output is directly proportional to the temperature difference of TEMs. According to Figs 6 (d1) and (d2), in the ATEG system with fins, the temperature differences of the four TEMs from the first to the last are 160 K, 151.87 K, 142.79 K, and 135.93 K, respectively, while in the ATEG system without fins, those are 102.03 K, 95.32 K, 90.59 K, 88.86 K, respectively. It seems that the use of fins can dramatically improve the temperature difference of TEMs. In this study, the optimal fin parameters reported in [32] are adopted. However, the heat exchanger parameters play an important role in the performance of the ATEG system, as well the fin parameters depend on the structure of the heat exchanger. Therefore, the optimal design of the heat exchanger is a priority and essential.

3.2 Pressure distributions

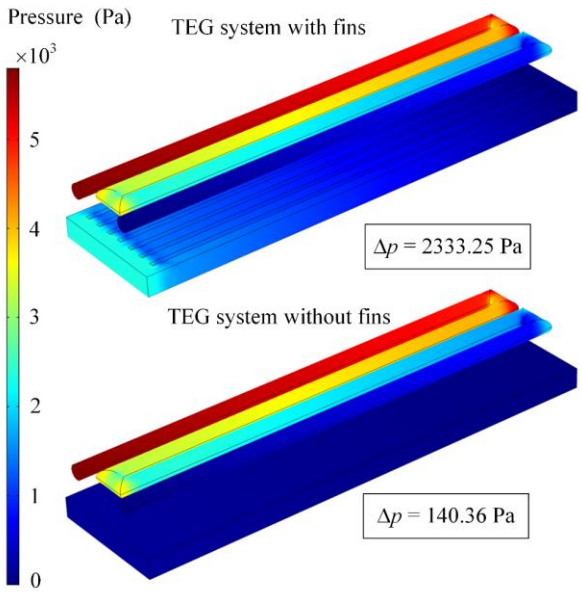

Fig. 7. Pressure distributions of the exhaust gas and cooling water.

Fig. 7 shows the pressure distributions of the exhaust gas and cooling water in the ATEG system.

The pressure drop of the cooling water is significantly greater than that of the exhaust gas. However, the backpressure loss of the exhaust gas is higher than the pumping power loss of the cooling water, due to the larger cross-sectional area of the exhaust gas channel and the larger velocity of the exhaust gas. The exhaust pressure drop in the ATEG system with fins (Δp = 2333.25 Pa) is greater than that in the ATEG system without fins (Δp = 140.36 Pa), because fins will block the exhaust flow and cause additional resistance. The exhaust pressure drop has a negative influence on the net power of the ATEG system. To avoid excessive pressure drop caused by the use of fins, the heat exchanger can be designed with a larger exhaust channel, but it may lead to inefficient heat transfer between the exhaust gas and the heat exchanger. Therefore, a set of optimal heat exchanger parameters should be selected to balance the pressure drop and heat transfer, including height, width, and length. Moreover, the optimal parameters of the heat exchanger with fins are different from those of the heat exchanger without fins.

3.3 Voltage distributions

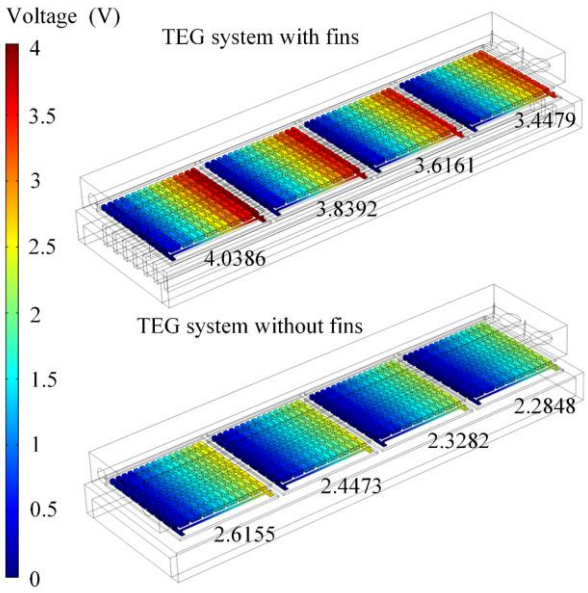

Fig. 8. Voltage distributions of the TEMs in the ATEG system.

Fig. 8 shows the voltage distributions of the TEMs. For a single TEM, the electric potential increases from cathode to anode due to the series connection of thermoelectric legs. In the ATEG system with fins, the output voltages of the four TEMs from the first to the last are 4.04 V, 3.84 V, 3.62 V, and 3.45 V, respectively, while in the ATEG system without fins, those are 2.62 V, 2.45 V, 2.33 V, and 2.28 V, respectively. The output voltage of the first TEM is the highest, and that of the last TEM is the lowest. In practical applications, all TEMs are usually connected in series, while the overall current of the ATEG system is limited by the smallest current among TEMs. Therefore, the length of the heat

exchanger should be controlled in a reasonable range. The more uniform the output voltage is, the smaller the power loss caused by the topological connection of TEMs will be.

As aforementioned, increasing the cross-sectional area of the exhaust channel is an effective way to reduce the exhaust pressure drop in the ATEG system with fins, which can be achieved by increasing the height and width of the heat exchanger. Fig. 9 shows voltage distributions of the TEMs under different widths for the ATEG system with fins. It can be observed that the total output voltage increases as the heat exchanger width (N_W) increases, because more TEMs are used to generate electricity. However, when N_W = 2 rows, the total output power of the ATEG system reaches the maximum, P_{out} = 17.12 W. With the increase of TEMs, the hot-side working temperature of TEMs decreases significantly, and the internal resistance of TEMs increases, resulting in a decrease in the overall power of the ATEG system. Note that the 1/2 structure is taken as the objective to predict the performance of the complete ATEG system herein, and the performance analysis in the following sections is based on the complete structure. Accordingly, the output power for the complete ATEG system is 34.24 W when N_W = 2 rows. The highest output power can not reflect the best performance of the ATEG system, and the conversion efficiency and power losses should also be considered. Besides, the heat exchanger with a fixed height of H = 15 mm is used in this section. When the height is different, the maximum output power may appear at a different heat exchanger width ($N_W \neq 2$ rows). To obtain the optimal design of the heat exchanger, a comprehensive analysis of the net power and net efficiency for the ATEG system with different parameters is performed in the following sections.

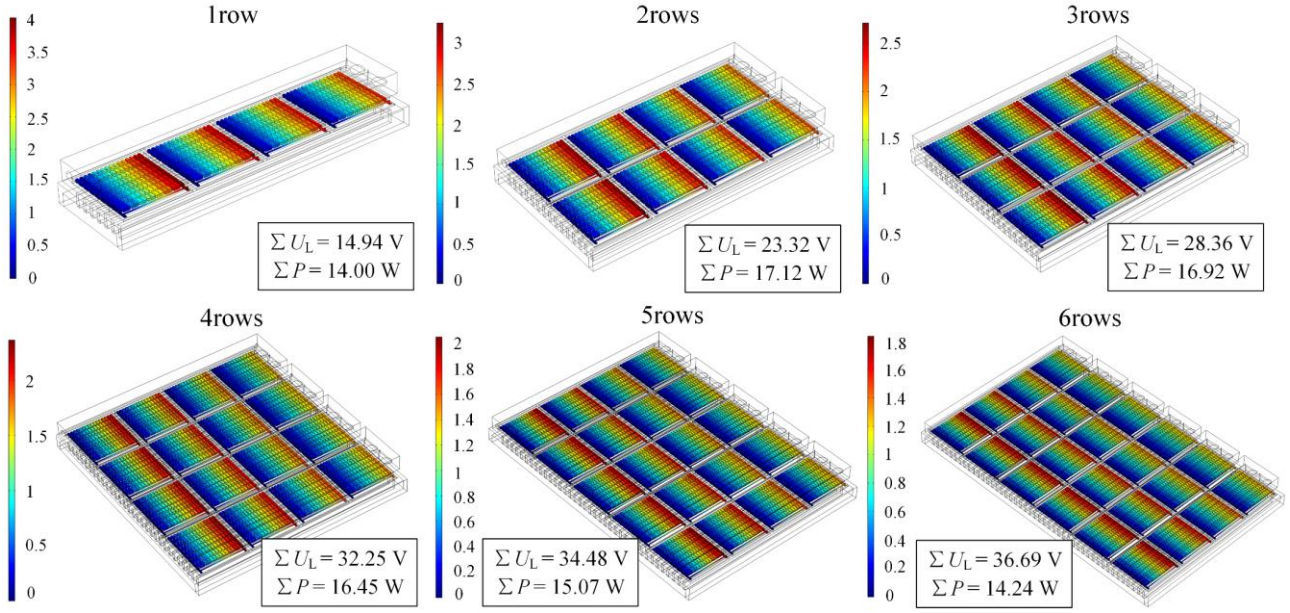

Fig. 9. Voltage distributions of the TEMs under different N_W for the ATEG system with fins.

4. Results and discussion

In determining the optimal parameters of the heat exchanger, both height and width affect the cross-sectional area of the exhaust channel, while the length only affects the length of the exhaust channel. Firstly, fixing the length (N_L = 4 columns), the height and width of the heat exchanger are optimized. Then, fixing the height and width, the length is optimized. Also, an index of the voltage uniformity is introduced to evaluate the performance, to avoid excessive power loss caused by the topological connection among TEMs. More importantly, the following selection criteria should be followed:

Criterion I: The net power and net efficiency of the ATEG system should be as high as possible.

Criterion II: Under the almost same net power or net efficiency, the height, width, and length of the heat exchanger should be as small as possible due to the space limitation of automobiles, especially the passenger car.

Criterion III: Under the almost same net power or net efficiency, TEMs should be used as little as possible, to reduce the cost.

4.1 Effect of the height and width on the performance of the ATEG system with fins

Fig. 10(a) shows the output power of the ATEG system at different widths and heights. Under the same width, the output power decreases with the increase in height, especially when the height is relatively low. The reason is that the lower the height is, the more intense the heat transfer between the exhaust gas and the heat exchanger is, and the higher the hot-side working temperature of TEMs will be. However, the situation for the heat exchanger width is quite different. The output power first increases and then decreases with the increase of width, and the optimal width seems to be N_W = 2 or 3 rows. When the width is at a relatively small value, the heat absorbed by the heat exchanger can not be effectively utilized by a few TEMs, and the output power can be further improved by applying more TEMs. With the further increase of the width, the increasing number of TEMs may lead to the excessive reduction of the heat allocated to each TEM, and can not balance the negative effect of the increase of internal resistance, resulting in the decrease of the total output power.

The output power can not be used as the only criterion to determine the optimal parameters of the heat exchanger, and the energy loss should also be considered. Fig. 10(b) shows the power losses of the ATEG system at different widths and heights. The backpressure loss decreases with the increase in height and width, especially when the height and width are relatively low. When the height and width of the heat exchanger are too small, the crowded exhaust flow will lead to a large backpressure loss. To achieve a small backpressure loss, the height should be greater than 15mm and the width

should be greater than 2 rows. Unlike the backpressure loss, the weight loss is proportional to the height and width of the heat exchanger, and the influence of the width is greater than that of the height. In addition, the pumping power loss is only affected by the width and is proportional to the width (not shown in the figure). However, compared with backpressure loss and weight loss, the pumping power loss is quite small. When the width increases from 1 row to 6 rows, the pumping power loss increases from 0.27 W to 1.63 W.

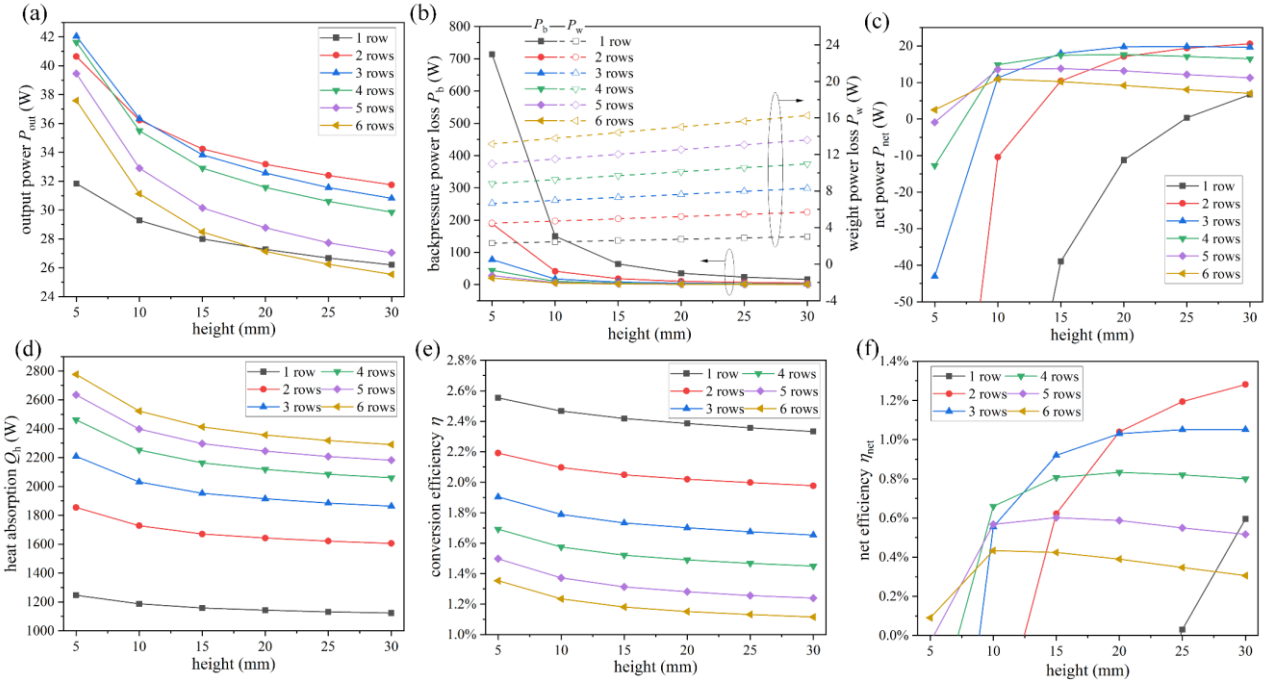

Fig. 10. Effect of the height and width on the performance of the ATEG system with fins. (a) Output power; (b) Power losses; (c) Net power; (d) Heat absorption; (e) Conversion efficiency; (f) Net efficiency.

Considering the backpressure loss, weight loss, and pumping power loss, the net power of the ATEG system is obtained, as shown in Fig. 10(c). It is worth noting that the extremely low width and height will produce negative gains for the ATEG system. The best working points can be observed at N_W = 3 rows (H = 20 mm, 25 mm, and 30 mm) and N_W = 2 rows (H = 25 mm and 30 mm). According to criteria I and II, the points of N_W = 3 rows (H = 25 mm and 30 mm) and N_W = 2 rows (H = 25 mm) are abandoned. The net power of the ATEG system is 19.73 W when N_W = 3 rows and H = 20 mm, and 20.58 W when N_W = 2 rows and H = 30 mm. According to criteria I and III, the heat exchanger with N_W = 2 rows and H = 30 mm is better than the heat exchanger with N_W = 3 rows and H = 20 mm, because it uses fewer TEMs and has a slightly higher net power.

Besides the net power, the conversion efficiency of the ATEG system is also an important index to determine the optimal design of the heat exchanger. Fig. 10(d) shows the heat absorption of the ATEG

system. The heat absorption increases with the increase of the width and the decrease of the height, and the influence of the width is greater than that of the height. The reason is that with the increase of the width, the heat transfer area increases, and the increasing number of TEMs leads to an increase in the heat demand from the exhaust gas. With the increase in height, although the heat transfer area increases slightly, the convective heat transfer coefficient between the exhaust gas and the heat exchanger decreases significantly, resulting in a decrease in heat absorption. Fig. 10(e) shows the conversion efficiency of the ATEG system. The conversion efficiency decreases with the increase of the width, which is opposite to the situation of the heat absorption because the conversion efficiency is inversely proportional to the heat absorption. However, with the increase in height, the conversion efficiency keeps the same change trend as the heat absorption, that is, it decreases, which is caused by the decrease of the output power.

Similarly, the ultrahigh conversion efficiency when N_W = 1 row can not represent the best performance of the ATEG system due to its excessive power losses. The net efficiency is more worthy to discuss. According to Fig. 10(f), it is obvious that when N_W = 2 rows and H = 30 mm, the net efficiency is the highest, which is 1.28%.

Based on the above analysis, the heat exchanger with N_W = 2 rows and H = 30 mm can achieve the best performance of the ATEG system with fins, with the output power of 31.75 W, the net power of 20.58 W, the conversion efficiency of 1.98%, and the net efficiency of 1.28%. In the previous studies [11], the conversion efficiency of the ATEG system is about 1.3% under a similar inlet exhaust temperature, which is significantly lower than 1.98% herein. It can be concluded that the conversion efficiency of the ATEG system can be effectively enhanced by optimizing the heat exchanger structure. According to Figs 10(c) and (f), it seems that the net power and net efficiency of the ATEG system can be further improved with the increase in height. Through the numerical simulation for the case of N_W = 2 rows and H = 35 mm, it is found that the net power, in this case, is the same as that in the case of N_W = 2 rows and H = 30 mm, although the net efficiency is slightly improved. Combined with criterion II, the optimal heat exchanger parameters of N_W = 2 rows and H = 30 mm are ultimately determined for the ATEG system with fins.

4.2 Effect of the height and width on the performance of the ATEG system without fins

A similar study is also carried out on the ATEG system without fins. Fig. 11(a) shows the output power of the ATEG system without fins. The variation of the output power with the height and width is almost the same as that in Fig. 10(a), except for the case of N_W = 1 row to N_W = 2 rows, due to the

small exhaust channel in the finned heat exchanger. Fig. 11(b) shows the power losses of the ATEG system without fins. Compared with Fig. 10(b), the only difference is that the amount of heat losses in the ATEG system without fins is smaller than that in the ATEG system with fins. Generally, the fins can enhance the heat transfer and improve the performance, but bring greater power losses to the ATEG system. It is necessary to determine reasonable fin parameters to balance the increased power and power loss, therefore, the optimal fin parameters previously reported are adopted in this work.

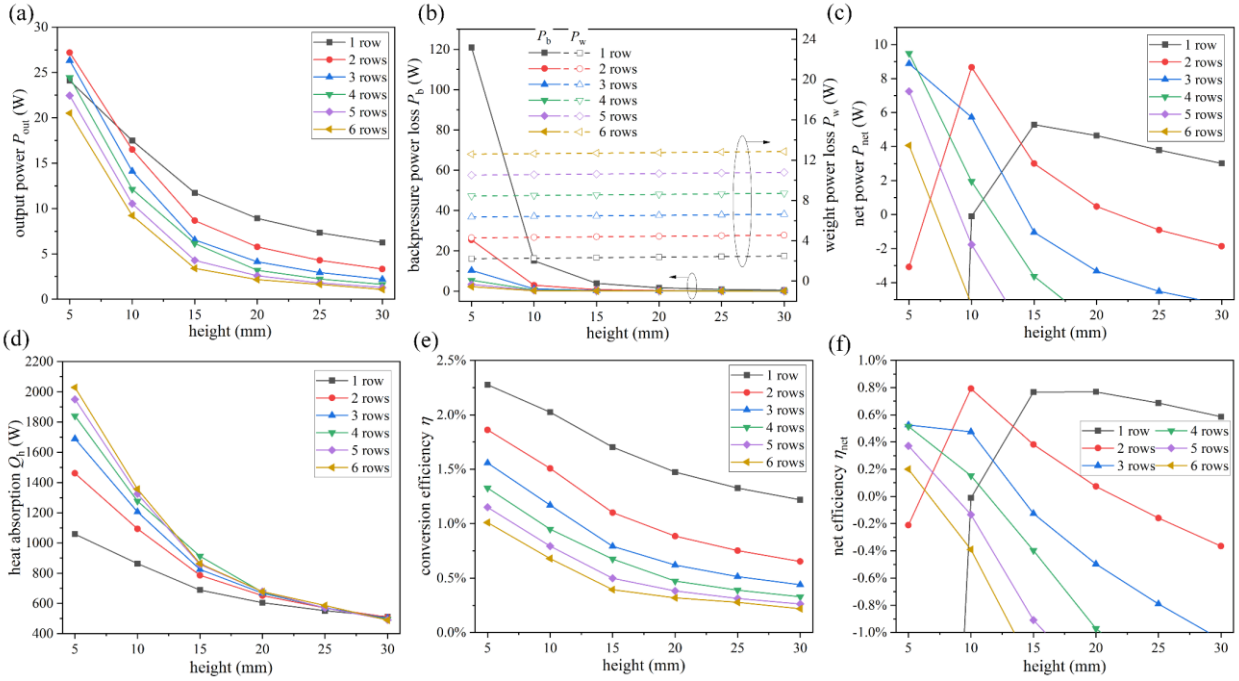

Fig. 11. Effect of the height and width on the performance of the ATEG system without fins. (a) Output power; (b) Power losses; (c) Net power; (d) Heat absorption; (e) Conversion efficiency; (f) Net efficiency.

Fig. 11(c) shows the net power of the ATEG system without fins. The optimal points of H = 5 mm (N_W = 3 rows and 4 rows) and H = 10 mm (N_W = 2 rows) can be observed. According to criterion III, the heat exchanger with H = 10 mm and N_W = 2 rows is preferred to the other two heat exchangers, because it uses fewer TEMs and has almost the same net power. Figs 11(d) and (e) show the heat absorption and conversion efficiency of the ATEG system without fins, respectively. The heat absorption decreases with the increase in height and the decrease in width. However, when the height reaches a relatively high value, that is $H \geq 25$ mm in this study, the influence of the width on the heat absorption becomes tiny because the heat transfer is close to saturation. The changing trend of the conversion efficiency of the ATEG system without fins is consistent with that of the ATEG system with fins in Fig. 10(e), but with a smaller conversion efficiency.

Fig. 11(f) shows the net efficiency of the ATEG system without fins. The results show that the heat

exchanger with H = 10 mm and N_W = 2 rows can not only achieve the optimal net power but also achieve the optimal net efficiency. When H = 10 mm and N_W = 2 rows, the output power, net power, conversion efficiency, and net efficiency of the ATEG system without fins are 16.49 W, 8.67 W, 1.51%, and 0.79%, respectively.

4.3 Voltage uniformity coefficient and the influence of the height and width on it

Accordingly, the optimal height and width for the heat exchangers with or without fins are obtained. However, the output power of the ATEG system is calculated based on the sum of the output power of each TEM, and the topological relationship among TEMs is ignored. The temperature differences of TEMs located in different positions of the heat exchanger are different. When all TEMs are connected in series, a parasitic power loss will occur due to the uneven output of TEMs. For this reason, a voltage uniformity coefficient is proposed to quantify this nonuniform output, which is defined by Eq. (20). Compared with the temperature uniformity coefficient proposed by Su et al. [25], the voltage uniformity coefficient can directly reveal the uneven output among TEMs.

$$\gamma = 1 - \frac{1}{N}\sum_{i=1}^{N}\frac{\sqrt{\left(U_i - U_{ave}\right)^2}}{U_{ave}} \tag{20}$$

where, N denotes the total number of TEMs used, i denotes the ith TEM, U_i represents the output voltage of the ith TEM, U_{ave} represents the average output voltage of all TEMs, respectively.

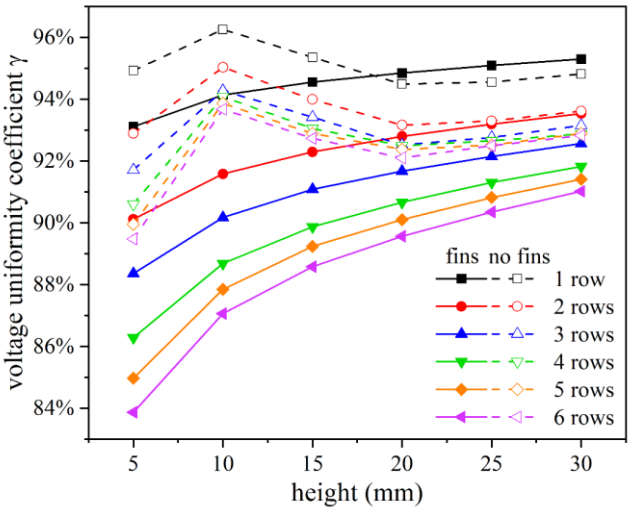

Fig. 12. Effect of the height and width on the voltage uniformity.

Fig. 12 shows the voltage uniformity coefficient of the ATEG system at different heights and widths. Under the same height, the voltage uniformity coefficient decreases with the increase of the width. The reason is that the larger the width of the heat exchanger is, the more TEMs are used in the ATEG

system. Therefore, the optimal width of N_W = 2 rows obtained above can not only achieve the best performance but also achieve a relatively high voltage uniformity coefficient. For the ATEG system with fins, the voltage uniformity coefficient increases with the increase in height. However, the situation for the ATEG system without fins is quite different. When H = 10 mm, the voltage uniformity coefficient reaches the highest value. Based on the above analysis, the optimal parameters (N_W = 2 rows and H = 30 mm for the heat exchanger with fins, and N_W = 2 rows and H = 10 mm for the heat exchanger without fins) are obtained, which can achieve high voltage uniformity and effectively reduce parasitic loss.

4.4 Effect of the length

Fig. 13(a) shows the output power, power losses, and net power of the ATEG system under different lengths. With the increase in the length, the output power, weight loss, backpressure loss, and pumping power loss increase, because more heat in the exhaust gas is reused by the increased length, and the increased length leads to the increase in power losses. However, the net power does not increase with the increase in the length. The reason is that the output power of the TEM decreases with the downward flow of the exhaust gas. If the length is too long, the increased power will be less than the increase in power losses. The optimal length of N_L = 4 columns for the heat exchanger without fins can be observed. In the case of the heat exchanger with fins, the net power can be further increased with the increase of the length ($N_L > 6$ columns). However, when the length is further increased, the net efficiency and voltage uniformity may be greatly reduced, thus affecting the performance of the ATEG system. These two factors should also be taken into account when determining the optimal length of the heat exchanger with fins.

Fig. 13(b) shows the net efficiency and voltage uniformity coefficient of the ATEG system under different lengths. Generally, the efficiency decreases with the increase in the length. With the increase of the length, more TEMs are used, and the conversion efficiency of a single TEM is reduced, resulting in the decline of the overall efficiency of the ATEG system. For the optimized heat exchanger without fins (N_W = 2 rows, H = 10 mm, and N_L = 4 columns), the conversion efficiency and net efficiency are 1.51% and 0.77% respectively. For the heat exchanger with fins, when $N_L \geq 4$ columns, the increase of the net power becomes more and more gentle, but the net conversion efficiency decreases constantly. It is difficult to determine its optimal length. Combined with the results of the voltage uniformity, when N_L = 5 columns and 6 columns, the voltage uniformity coefficients of the ATEG system with fins are 0.901 and 0.862 respectively, and the output voltages of the TEM in the last column are

respectively 76% and 67% of those of the TEM in the first column. When all TEMs are connected in series, through a simple calculation, the power penalty caused by increasing the length from N_L = 5 columns to 6 columns is greater than the corresponding power increment. However, even if the voltage uniformity coefficient decreases from 0.998 to 0.901, the output power of the ATEG system still increases as N_L increases from 1 column to 5 columns. Herein, the voltage uniformity coefficient is suggested to be higher than 0.9. Therefore, the optimal heat exchanger with fins (N_W = 2 rows, H = 30 mm, and N_L = 5 columns) is obtained, with the output power of 35.49 W, the net power of 22.93 W, the conversion efficiency of 1.89%, and the net efficiency of 1.22%. Compared with the optimal ATEG system without fins, the net power and net efficiency of the optimal one with fins are increased by 164.48% and 54.43% respectively. In Ref. [50], the developed ATEG system (N_W = 2 rows, H = 20 mm, and N_L = 5 columns) with winglets could deliver the maximum conversion efficiency of 1.2% under similar conditions, which is lower than the maximum efficiency of 1.89% of the ATEG system with the optimal design.

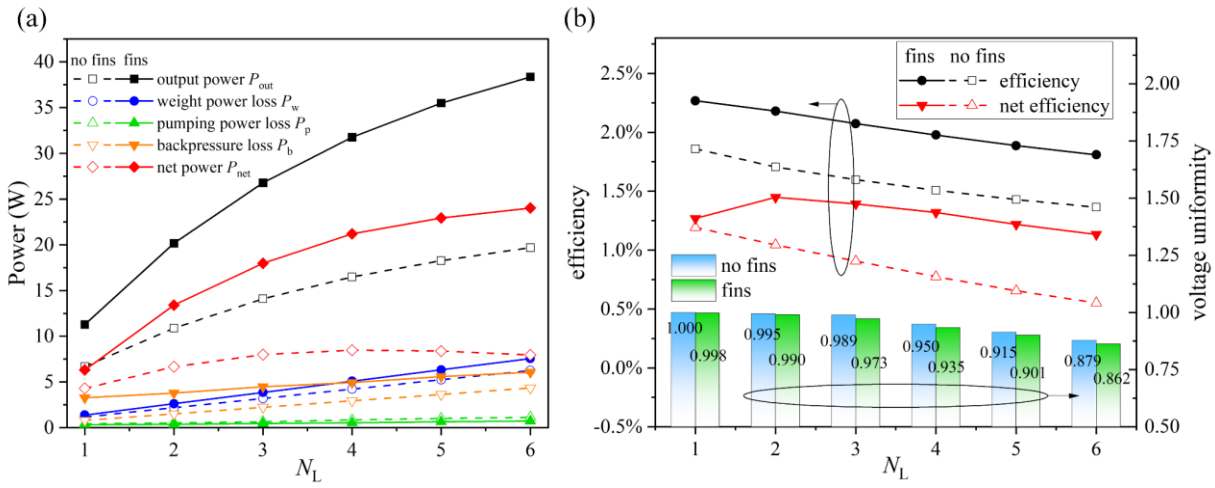

Fig. 13. Effect of the length on the performance of the ATEG system. (a) Output power, power losses, and net power; (b) Efficiency, net efficiency, and voltage uniformity.

5. Conclusions

In this study, a fluid-thermal-electric multiphysics model is used to optimize the heat exchanger of the ATEG system for a passenger car. A net power model of the ATEG system is also established to comprehensively evaluate the performance of the ATEG system, with the consideration of weight loss, backpressure loss, and pumping power loss. According to the numerical results, the height, width, and length of the heat exchanger are optimized. Besides, the optimal parameters of two kinds of heat exchangers with and without fins are determined, and the performance of the two kinds of heat

exchangers is compared. The main conclusions can be drawn as follows:

(1) The fluid-thermal-electric multiphysics numerical model, considering the actual working conditions of the ATEG system, can obtain accurate distribution characteristics of the fluid, thermal, and electric fields. The model provides a new tool to guide the optimization of automotive thermoelectric generators. Through experimental validation, the average errors of output voltage and power between experimental and model results are 1.42% and 2.81% respectively.

(2) The output power and conversion efficiency of the ATEG system can be improved by reducing the cross-sectional area of the heat exchanger, but the power loss, especially the backpressure loss, also increases. With the increase in the length of the heat exchanger, the output power increases, whereas the conversion efficiency decreases. It is necessary to consider the power loss caused by the ATEG system, and use the net power and net efficiency as optimization objectives to optimize its structure parameters.

(3) The voltage uniformity coefficient decreases with the increases in the width and length. When the length increases from N_L = 5 columns to 6 columns, the voltage uniformity coefficient of the ATEG system with fins decreases from 0.901 to 0.862, and when all TEMs are connected in series, the power penalty caused by increasing the length from N_L = 5 columns to 6 columns is greater than the corresponding power increment. To avoid excessive parasitic loss, it is suggested that the voltage uniformity coefficient should be greater than 0.9.

(4) Through optimization, the optimal parameters of N_W = 2 rows, H = 30 mm, and N_L = 5 columns for the heat exchanger with fins, and those of N_W = 2 rows, H = 10 mm, and N_L = 4 columns for the heat exchanger without fins are obtained. The output power, net power, conversion efficiency, and net efficiency of the optimal ATEG system with fins are 35.49 W, 22.93 W, 1.89%, and 1.22%, respectively, and those of the optimal ATEG system without fins are 16.49 W, 8.67 W, 1.51%, and 0.79%, respectively. The net power and net efficiency of the ATEG system can be increased by 164.48% and 54.43% respectively by using fins.

Acknowledgements

This work was supported by the National Natural Science Foundation of China (52072217 and 22179071), and the Major Technological Innovation Project of Hubei Science and Technology Department (2019AAA164).

References

[1] Shen Z-G, Tian L-L, Liu X. Automotive exhaust thermoelectric generators: Current status, challenges and future prospects. Energy Convers Manage 2019;195:1138-73.
[2] Twaha S, Zhu J, Yan Y, Li B. A comprehensive review of thermoelectric technology: Materials, applications, modelling and performance improvement. Renewable Sustainable Energy Rev 2016;65:698-726.
[3] Luo D, Yan Y, Li Y, Wang R, Cheng S, Yang X, et al. A hybrid transient CFD-thermoelectric numerical model for automobile thermoelectric generator systems. Appl Energy 2023;332:120502.
[4] Zhang Y. Thermoelectric Advances to Capture Waste Heat in Automobiles. ACS Energy Letters. 2018;3:1523-4.
[5] Risseh AE, Nee H-P, Goupil C. Electrical Power Conditioning System for Thermoelectric Waste Heat Recovery in Commercial Vehicles. IEEE Transactions on Transportation Electrification. 2018;4:548-62.
[6] Brito FP, Pacheco N, Vieira R, Martins J, Martins L, Teixeira J, et al. Efficiency improvement of vehicles using temperature controlled exhaust thermoelectric generators. Energy Convers Manage 2020;203:112255.
[7] Zhao Y, Lu M, Li Y, Wang Y, Ge M. Numerical investigation of an exhaust thermoelectric generator with a perforated plate. Energy. 2023;263:125776.
[8] Ge M, Li Z, Zhao Y, Xuan Z, Li Y, Zhao Y. Experimental study of thermoelectric generator with different numbers of modules for waste heat recovery. Appl Energy 2022;322:119523.
[9] Lan S, Stobart R, Chen R. Performance comparison of a thermoelectric generator applied in conventional vehicles and extended-range electric vehicles. Energy Convers Manage 2022;266:115791.
[10] Lan S, Yang Z, Chen R, Stobart R. A dynamic model for thermoelectric generator applied to vehicle waste heat recovery. Appl Energy 2018;210:327-38.
[11] Kim TY, Kwak J, Kim B-w. Energy harvesting performance of hexagonal shaped thermoelectric generator for passenger vehicle applications: An experimental approach. Energy Convers Manage 2018;160:14-21.
[12] Crane D, LaGrandeur J, Jovovic V, Ranalli M, Adldinger M, Poliquin E, et al. TEG On-Vehicle Performance and Model Validation and What It Means for Further TEG Development. J Electron Mater 2013;42:1582-91.
[13] Luo D, Zhao Y, Yan Y, Chen H, Chen W-H, Wang R, et al. Development of two transient models

for predicting dynamic response characteristics of an automobile thermoelectric generator system. Appl Therm Eng 2023;221:119793.
[14] Wan Q, Liu X, Gu B, Bai W, Su C, Deng Y. Thermal and acoustic performance of an integrated automotive thermoelectric generation system. Appl Therm Eng 2019;158:113802.
[15] Yang H, Shu G, Tian H, Ma X, Chen T, Liu P. Optimization of thermoelectric generator (TEG) integrated with three-way catalytic converter (TWC) for harvesting engine's exhaust waste heat. Appl Therm Eng 2018;144:628-38.
[16] Wu Y, Yang J, Chen S, Zuo L. Thermo-element geometry optimization for high thermoelectric efficiency. Energy. 2018;147:672-80.
[17] Agudelo AF, García-Contreras R, Agudelo JR, Armas O. Potential for exhaust gas energy recovery in a diesel passenger car under European driving cycle. Appl Energy 2016;174:201-12.
[18] Yu G, Shu G, Tian H, Wei H, Liu L. Simulation and thermodynamic analysis of a bottoming Organic Rankine Cycle (ORC) of diesel engine (DE). Energy. 2013;51:281-90.
[19] Wang Y, Li S, Xie X, Deng Y, Liu X, Su C. Performance evaluation of an automotive thermoelectric generator with inserted fins or dimpled-surface hot heat exchanger. Appl Energy 2018;218:391-401.
[20] Yan S-R, Moria H, Asaadi S, Sadighi Dizaji H, Khalilarya S, Jermsittiparsert K. Performance and profit analysis of thermoelectric power generators mounted on channels with different cross-sectional shapes. Appl Therm Eng 2020:115455.
[21] Fernández-Yañez P, Armas O, Capetillo A, Martínez-Martínez S. Thermal analysis of a thermoelectric generator for light-duty diesel engines. Appl Energy 2018;226:690-702.
[22] Cao Q, Luan W, Wang T. Performance enhancement of heat pipes assisted thermoelectric generator for automobile exhaust heat recovery. Appl Therm Eng 2018;130:1472-9.
[23] Pacheco N, Brito FP, Vieira R, Martins J, Barbosa H, Goncalves LM. Compact automotive thermoelectric generator with embedded heat pipes for thermal control. Energy. 2020;197:117154.
[24] Bai S, Lu H, Wu T, Yin X, Shi X, Chen L. Numerical and experimental analysis for exhaust heat exchangers in automobile thermoelectric generators. Case Studies in Thermal Engineering. 2014;4:99-112.
[25] Su CQ, Huang C, Deng YD, Wang YP, Chu PQ, Zheng SJ. Simulation and Optimization of the Heat Exchanger for Automotive Exhaust-Based Thermoelectric Generators. J Electron Mater 2016;45:1464-72.

[26] Chen W-H, Lin Y-X, Chiou Y-B, Lin Y-L, Wang X-D. A computational fluid dynamics (CFD) approach of thermoelectric generator (TEG) for power generation. Appl Therm Eng 2020;173:115203.
[27] Luo D, Wang R, Yu W, Zhou W. A novel optimization method for thermoelectric module used in waste heat recovery. Energy Convers Manage 2020;209:112645.
[28] Luo D, Wang R, Yu W. Comparison and parametric study of two theoretical modeling approaches based on an air-to-water thermoelectric generator system. J Power Sources 2019;439:227069.
[29] Kempf N, Zhang Y. Design and optimization of automotive thermoelectric generators for maximum fuel efficiency improvement. Energy Convers Manage 2016;121:224-31.
[30] Luo D, Wang R. Experimental Test and Estimation of the Equivalent Thermoelectric Properties for a Thermoelectric Module. J Energy Res Technol 2021;143:122102.
[31] Chen W-H, Liao C-Y, Hung C-I, Huang W-L. Experimental study on thermoelectric modules for power generation at various operating conditions. Energy. 2012;45:874-81.
[32] Vale S, Heber L, Coelho PJ, Silva CM. Parametric study of a thermoelectric generator system for exhaust gas energy recovery in diesel road freight transportation. Energy Convers Manage 2017;133:167-77.
[33] Marvão A, Coelho PJ, Rodrigues HC. Optimization of a thermoelectric generator for heavy-duty vehicles. Energy Convers Manage 2019;179:178-91.
[34] Wang S, Xie T, Xie H. Experimental study of the effects of the thermal contact resistance on the performance of thermoelectric generator. Appl Therm Eng 2018;130:847-53.
[35] Luo D, Wang R, Yan Y, Yu W, Zhou W. Transient numerical modelling of a thermoelectric generator system used for automotive exhaust waste heat recovery. Appl Energy 2021;297:117151.
[36] Li Y, Shi Y, Wang X, Luo D, Yan Y. Thermal and electrical contact resistances of thermoelectric generator: Experimental study and artificial neural network modelling. Appl Therm Eng 2023;225:120154.
[37] Anderson JD, Wendt J. Computational fluid dynamics: Springer; 1995.
[38] Nithyanandam K, Mahajan RL. Evaluation of metal foam based thermoelectric generators for automobile waste heat recovery. Int J Heat Mass Transfer 2018;122:877-83.
[39] Fluent A. Fluent 14.0 user's guide2011.
[40] Meng J-H, Wu H-C, Gao D-Y, Kai Z, Lu G, Yan W-M. A novel super-cooling enhancement method for a two-stage thermoelectric cooler using integrated triangular-square current pulses.

Energy. 2021;217:119360.
[41] Luo D, Liu Z, Yan Y, Li Y, Wang R, Zhang L, et al. Recent advances in modeling and simulation of thermoelectric power generation. Energy Convers Manage 2022;273:116389.
[42] Meng J-H, Wu H-C, Wang L, Lu G, Zhang K, Yan W-M. Thermal management of a flexible controlled thermoelectric energy conversion-utilization system using a multi-objective optimization. Appl Therm Eng 2020;179:115721.
[43] Wipke KB, Cuddy MR, Burch SD. ADVISOR 2.1: a user-friendly advanced powertrain simulation using a combined backward/forward approach. IEEE Trans Veh Technol 1999;48:1751-61.
[44] Karri MA, Thacher EF, Helenbrook BT. Exhaust energy conversion by thermoelectric generator: Two case studies. Energy Convers Manage 2011;52:1596-611.
[45] Luo D, Wang R, Yu W, Zhou W. Performance optimization of a converging thermoelectric generator system via multiphysics simulations. Energy. 2020;204:117974.
[46] Liu X, Zhang C-F, Zhou J-G, Xiong X, Wang Y-P. Thermal performance of battery thermal management system using fins to enhance the combination of thermoelectric Cooler and phase change Material. Appl Energy 2022;322:119503.
[47] Luo D, Wang R, Yu W, Zhou W. Parametric study of a thermoelectric module used for both power generation and cooling. Renewable Energy 2020;154:542-52.
[48] Liu K, Tang X, Liu Y, Xu Z, Yuan Z, Li J, et al. Preparation and optimization of miniaturized radioisotope thermoelectric generator based on concentric filament architecture. J Power Sources 2018;407:14-22.
[49] Wang T, Luan W, Liu T, Tu S-T, Yan J. Performance enhancement of thermoelectric waste heat recovery system by using metal foam inserts. Energy Convers Manage 2016;124:13-9.
[50] Lu X, Yu X, Qu Z, Wang Q, Ma T. Experimental investigation on thermoelectric generator with non-uniform hot-side heat exchanger for waste heat recovery. Energy Convers Manage 2017;150:403-14.